3-2021

A Hybrid Droplet Vaporization-Adaptive Surrogate Model Using an Optimized Continuous Thermodynamics Distribution

Simcha L. Singer
Marquette University, simcha.singer@marquette.edu

Michael Hayes
Marquette University

Alanna Y. Cooney
Marquette University

Fuel, Vol. 288 (March 2021): 119821. DOI.

A Hybrid Droplet Vaporization-Adaptive Surrogate Model Using an Optimized Continuous Thermodynamics Distribution

Simcha Singer
Department of Mechanical Engineering, Marquette University, Milwaukee, WI
Michael P. Hayes
Department of Mechanical Engineering, Marquette University, Milwaukee, WI
Alanna Y. Cooney
Department of Mechanical Engineering, Marquette University, Milwaukee, WI

Abstract

Liquid transportation fuels are composed of hundreds of species, necessitating the use of surrogates in CFD simulations. Surrogates composed of a few species are often formulated to emulate the combustion properties targets (CPTs) of pre-vaporized fuels but fail to reproduce their vaporization behavior, implying that such surrogates cannot replicate the CPTs in the presence of preferential vaporization. The prevailing approach to this problem proposes a physical–chemical surrogate formulated to match the fuel's distillation curve in addition

to its CPTs. However, the physical–chemical surrogate approach requires more species, may not reproduce the instantaneous (distillation-resolved) CPTs, and is not well-suited to conditions in which non-surrogate species surround the droplets. A recent hybrid approach addresses these shortcomings by combining a continuous thermodynamic model (CTM) for droplet vaporization with an adaptive chemical surrogate formulated using functional group matching (FGM). Whereas the hybrid model previously required a delumping calculation to recover discrete fluxes prior to FGM, the approach is modified here to directly predict the fluxes of functional groups using the CTM, increasing its flexibility for high-pressure applications. To this end, a novel, purely mathematical distribution variable is proposed to correlate key functional groups, in addition to thermophysical and transport properties. The accuracy and flexibility of both hybrid approaches compare favorably with the physical–chemical surrogate method. While droplet vaporization rates are well-represented by both methods, functional group fluxes and instantaneous CPTs are predicted more accurately by the hybrid methods, illustrating their potential for improving the accuracy of Eulerian-phase solvers in the presence of preferential vaporization.

Keywords

Multicomponent droplet vaporization, Surrogate, Combustion property targets, Continuous thermodynamics, Preferential vaporization

Nomenclature

B_M Spalding mass transfer number
B_T Spalding heat transfer number
C molar concentration
C_1, C_2… fitting constants
c_p specific heat capacity
D diffusion coefficient
f function
F objective function
I distribution variable
k thermal conductivity
l_v latent heat of vaporization
m moment
MW molecular weight
N number of CA-DQMoM nodes
Nu Nusselt number
n number of discrete species
$\dot{n}$ molar flow rate
r radial coordinate
R radius of droplet
R^2 coefficient of determination
R_f radius of gas film
S source term in CTM species equation
$\bar{S}$ source term in moment transformed species equation
Sh Sherwood number
T temperature
$\bar{T}$ volume averaged temperature
t time

w CA-DQMoM weight
$\bar{w}$ CA-DQMoM average weight
x mole fraction
$\bar{x}$ volume averaged mole fraction
δ delta function
ϕ fugacity coefficient
ρ density

Superscripts

$*$ modified (Sherwood number, Nusselt number)
i discrete species index
j CA-DQMoM node index
k moment order index
tot total (for all species)
ζ flux

Subscripts

g gas
i discrete species index
j CA-DQMoM node index
k moment order index
l liquid
nb normal boiling
s evaluated at droplet surface
v vapor
∞ at far-field boundary

Acronyms

CA-DQMoM Couple Algebraic-Direct Quadrature Method of Moments
CFD Computational Fluid Dynamics
CPT Combustion Property Target
CTM Continuous Thermodynamic Model
DCM Discrete Component Model
DCN Derived Cetane Number
DDFS Direct Dual Fuel Stratification
DQMoM Direct Quadrature Method of Moments
FGM Functional Group Matching
H/C Hydrogen to Carbon ratio
MW Molecular Weight
ODE Ordinary Differential Equation
QMoM Quadrature Method of Moments
RCCI Reactivity Controlled Compression Ignition
TSI Threshold Sooting index

1. Introduction

Liquid transportation fuels are typically comprised of hundreds of hydrocarbon species. Computational fluid dynamics (CFD) simulations for spray combustion in gasoline, jet and diesel engines must simplify the representation of these multicomponent fuels to achieve computational tractability. Surrogate mixtures composed of fewer species are therefore used to emulate the combustion behavior of real fuels. However, because surrogates have often been formulated to mimic the combustion properties of fully pre-vaporized fuels, they cannot account for the effects of preferential vaporization on combustion behavior [1], [2]. Recent findings that combustion properties are convergent for large hydrocarbon mixtures typical of transportation fuels [3] underscore the importance of capturing the impacts of the multicomponent nature of these fuels on droplet vaporization, physical properties and preferential vaporization [3], [4].

The prevailing approach to the address the problem of preferential vaporization employs a surrogate that can reproduce the fuel's distillation curve, in addition to its combustion property targets (CPTs) [5], [6], [7]. However, there are drawbacks to the physical–chemical surrogate approach. First, formulating a surrogate that accurately emulates the fuel's distillation curve in addition to its CPTs requires a significantly larger surrogate, increasing the computational cost for the Eulerian-phase solver. For instance, a 14-component physical–chemical surrogate was used to match the CPTs as well as the distillation curve for Jet-A [8]. Elsewhere, the combustion property targets of Jet-A were replicated using a four-species surrogate, but a nine-species surrogate was required to emulate its distillation curve [5].

Second, implicit in the physical–chemical surrogate approach is the assumption that matching the target fuel's distillation curve ensures that the behavior of a vaporizing surrogate droplet will match the behavior of the real droplets at engine-relevant conditions. However, the (advanced) distillation curve represents idealized, vapor–liquid equilibrium behavior [9], whereas multicomponent droplet vaporization is a more complex, partiallytransport-limited phenomenon. In other words, matching the distillation curve to a certain level of accuracy does not guarantee that the droplet vaporization behavior will be reproduced equally well. Furthermore, even if a physical–chemical surrogate is formulated to match the fuel's distillation curve in addition to its CPTs, this does not ensure that the instantaneous (distillation-resolved) chemical properties of the evaporated fuel will match that of the target fuel. This point has been noted by Wang et al. [4] in discussing the surrogate approach.

A third drawback associated with the physical–chemical surrogate approach is that it is not well-suited to accommodate conditions in which species other than the surrogate components surround the droplets and may even condense from the vapor phase [10]. For example, in a dual-fuel combustion environment, such as reactivity controlled compression ignition (RCCI) [11], a physical–chemical surrogate used to represent one fuel cannot straightforwardly accommodate the presence of the chemical species comprising the other fuel. Similarly, pyrolysis chemistry can produce hydrocarbon species (e.g. alkenes) present in the droplet boundary conditions that cannot be straightforwardly accommodated using a physical–chemical surrogate for the fuel.

A recently developed hybrid droplet vaporization–adaptive surrogate model employs a different approach to emulating the behavior of multicomponent liquid droplets and surrogate formulation [12]. Droplet vaporization and physical properties are modeled in a continuous thermodynamic framework using the Coupled Algebraic Direct Quadrature Method of Moments (CA-DQMoM) [13], rather than with a discrete surrogate. A Functional Group Matching (FGM) model is then used to determine the instantaneous vaporization flux of a small chemical surrogate composed of a few discrete species, which serves as the source term for the Eulerian phase. FGM adjusts the instantaneous chemical surrogate composition to ensure that the distribution of key functional groups in the flux from the droplet matches that of the chemical surrogate [12]. The hybrid method is a computationally efficient approach that emulates the physical properties, as well as the distillation resolved

CPTs, of a multicomponent fuel and provides a means to account for the effects of preferential vaporization on combustion behavior.

This hybrid approach differs from previous [14], [15] and subsequent [16] models that lumped large physical surrogates into smaller chemical surrogates. Whereas Krishnasamy et al. [14] linked a 14-component physical/spray surrogate to a 4-component chemical surrogate using a group chemistry representation based on hydrocarbon class, the hybrid method [12] generates the chemical surrogate to match the instantaneous distribution of functional groups in the vaporization flux from a droplet, since the distribution of functional groups has been shown to be a good predictor of combustion behavior [5]. The hybrid method [12] also differs from a subsequent approach [16] which appears to partially match functional groups, but it is not clear if the functional group distributions remain the same and if the matching is based on the instantaneous flux from the droplets. The hybrid model [12] is distinct from both approaches [14], [15], [16], [17] in that it uses a continuous thermodynamic model (CTM) to represent the droplet's vaporization and physical properties, rather than a discrete physical surrogate. CTMs using quadrature-based moment methods can be more flexible than discrete component models (DCMs) and their computational efficiency is not directly dependent on the number of physical surrogate components needed to represent a particular fuel and combustion environment.

The unified treatment of droplet vaporization and surrogate formulation ("the hybrid model") can circumvent the three shortcomings associated with the prevailing physical–chemical surrogate approach. CA-DQMoM treats a multicomponent mixture as a continuous distribution capable of assuming an arbitrary form. In contrast to physical–chemical surrogates, which generate Eulerian-phase source terms that consist of many discrete species, FGM produces a smaller, chemical surrogate for the Eulerian-phase solver. Furthermore, it will be shown in Section 3.4 that the hybrid droplet vaporization-adaptive surrogate model produces a more accurate solution for the instantaneous functional group fluxes and CPTs than a physical–chemical surrogate formulated to match the CPTs and the distillation curve of the same target fuel. Finally, in contrast to discrete physical–chemical surrogates, the CA-DQMoM approach can accommodate droplet boundary conditions that include species not present in the combined physical–chemical surrogate, which may even condense on the droplets under engine-relevant conditions [10], [18].

The previous version of the hybrid droplet vaporization-adaptive surrogate model [12] is depicted schematically in Fig. 1. It is noted that the continuous representation of the multicomponent mixture calculated by CA-DQMoM is "delumped" to produce a full discrete distribution, such that the flux of functional groups in the discrete fuel can be calculated and used to determine the composition of the surrogate flux using FGM. While providing high accuracy, this intermediate delumping step requires that any nonlinearity in the governing species equations be confined to terms associated with the mixture as a whole [19]. Although this condition is satisfied for many droplet vaporization models appropriate for use in CFD codes, applications to high-pressures and transcritical conditions characteristic of diesel or jet engines may require the incorporation of models that violate this condition, such as non-ideal Maxwell-Stefan transport models. Elimination of the delumping step would therefore facilitate application of the hybrid droplet vaporization-adaptive surrogate model to conditions encountered in high-pressure applications.

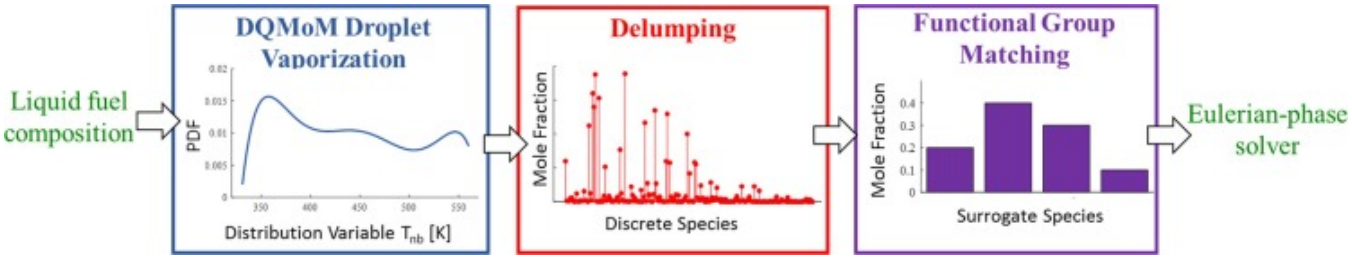

Fig. 1. Schematic depiction of the previous hybrid droplet vaporization – adaptive surrogate method.

The goals of this paper are, therefore: (1) to modify the hybrid droplet vaporization – adaptive surrogate approach by removing the intermediate delumping step in Fig. 1, and (2) to compare the accuracy of the hybrid approach, with and without delumping, to the prevailing physical–chemical surrogate approach. The CA-DQMoM droplet vaporization model will first be modified to directly predict the vaporization (condensation) fluxes of key functional groups from (to) the droplet, eliminating the need for the delumping submodel. Because typical continuous distributions variables are unable to correlate chemical functional groups in addition to the usual thermophysical properties, a novel, purely mathematical distribution variable is proposed. The idea of tailoring the CTM distribution variable to the desired model outputs can be applied to other chemical engineering problems and is not limited to CTMs using quadrature-based moment methods. Like the previous hybrid model with delumping, the functional group fluxes predicted directly by CA-DQMoM with the optimized distribution are then input to the Functional Group Matching (FGM) model to produce a time-dependent, distillation-resolved flux of surrogate species that can be input to the gas-phase CFD solver. In Section 2, the hybrid droplet vaporization model, including CA-DQMoM and FGM, will be summarized and the optimized distribution approach will be outlined. The dependence of thermophysical properties, transport properties and chemical functional groups on the optimized distribution variable will also be presented. In Section 3, the hybrid droplet vaporization-adaptive surrogate method using the optimized distribution will be compared to the hybrid model with delumping and to the physical–chemical surrogate approach. The accuracy of the three methods will be evaluated by comparing droplet vaporization behavior, functional group fluxes and CPTs to those predicted by the full discrete model for the multicomponent target fuel. Discussion of the results and conclusions will be considered in Section 4.

2. Droplet vaporization/adaptive surrogate model

2.1. Discrete component model

The hybrid approach can be applied to a variety of physical models for multicomponent droplet vaporization. The particular discrete component model (DCM) upon which the present CTM is based has been described previously [13], but has been modified [20] to incorporate the Peng-Robinson equation of state [21]. The droplets are assumed to be spherically symmetric. To account for finite rates of liquid mass transfer [22], governing differential and algebraic equations are solved for the volume averaged mole fractions, $\bar{x}_l^i$, and surface mole fractions, xl,si, of all *n* species comprising the droplet:

(1)

$$\frac{d\bar{x}_l^i}{dt} = \left(\frac{15D_l}{R^2} + \frac{3}{R}\frac{dR}{dt}\right)\left(x_{ls}^i - \bar{x}_l^i\right)$$

(2)

$$x_{l,s}^i = \frac{5C_lD_l\bar{x}_l^i + \frac{C_gD_gSh_g^*ln(1+B_M)}{2B_M}x_{g,\infty}^i}{5C_lD_l + C_lR\frac{dR}{dt}\left(1 - \frac{\phi_{l,s}^i}{\phi_{g,s}^i}\right) + \frac{C_gD_gSh_g^*ln(1+B_M)}{2B_M}\frac{\phi_{l,s}^i}{\phi_{g,s}^i}}$$

The symbols appearing in the equations are listed in the nomenclature and are generally standard.

As in all sub-grid-scale droplet models appropriate for Lagrangian-Eulerian CFD codes, transport in the gas-phase boundary layer surrounding the droplet is assumed to be quasi-steady [23]. A mass balance at the droplet surface yields the expression for the rate of change of droplet size

(3)

$$\frac{dR}{dt} = -\frac{C_g D_g Sh_g^* ln(1+B_M)}{2C_l R}$$

where the Spalding transfer number on a molar basis is defined

(4)

$$B_M = \frac{x_{g,s}^{tot} - x_{g,\infty}^{tot}}{1 - x_{g,s}^{tot}}$$

and the modified Sherwood number is defined [23]:

(5)

$$Sh_g^* = \frac{B_M}{ln(1+B_M)} Sh_g$$

The total molar vaporization rate is given by

(6)

$$\dot{n}^{tot} = 2\pi R C_g D_g Sh_g^* ln(1+B_M)$$

and the vapor molar flow rate of each discrete species, which would serve as the source term for the Eulerian phase, is:

(7)

$$\dot{n}^i = \dot{n}^{tot} \frac{\left(x_{g,s}^i (1+B_M) - x_{g,\infty}^i\right)}{B_M}$$

While previous versions of the hybrid model employed the ideal gas equation of state and Raoult's Law for vapor–liquid equilibrium at the interface, the Peng-Robinson equation of state [21] and non-ideal vapor–liquid equilibrium are employed at present and have been incorporated in Eq. (2), where the fugacity coefficient for each species, *i*, and phase, *p*, is ϕ_p^i. The binary interaction coefficients for hydrocarbon pairs are assumed to be zero.

The species equations above can be coupled with a variety of approaches for calculating the droplet temperature, including infinite conductivity, quasi-steady and effective conductivity models [24]. In this paper, the liquid temperature within the droplet was modeled with a parabolic temperature profile [25] using equations for the droplet's average, $\bar{T}_l$, and surface, $T_{l,s}$, temperature [26]:

(8)

$$\frac{d\bar{T}_l}{dt} = \frac{3}{2} \frac{k_g Nu_g^* ln(1+B_T)}{C_l c_{p,l} R^2 B_T \left(1 + \frac{1}{10}\left(\frac{k_g Nu_g^* ln(1+B_T)}{k_l B_T}\right)\right)} \left(T_\infty - \frac{B_T l_v}{c_{p,v}} - \bar{T}_l\right)$$

(9)

$$T_{l,s} = \bar{T}_l + \frac{R^2 C_l c_{p,l}}{15 k_l} \frac{d\bar{T}_l}{dt}$$

The Spalding heat transfer number [23], [26] is given by

(10)

$$B_T = (1 + B_M)^{(D_g \rho_g c_{p,v})/(k_g MW_g)} - 1$$

and the modified Nusselt number, Nu_g^*, [26] is defined in a similar manner to the modified Sherwood number. The latent heat of vaporization of the mixture, l_v, and the heat capacity of the vapor, $c_{p,v}$, are found using flux weighted mixing equations, which will be discussed in Section 2.2.2. The need for flux weighting of the discrete properties in these equations is discussed by Laurent [26]. Temperature-dependent thermophysical and transport properties for all the discrete species are obtained from the Yaws' database [27]. Properties for the gas-phase are evaluated using the 1/3 rule [28].

Discrete component models are the most accurate approach for representing the multicomponent nature of droplet vaporization but are computationally prohibitive for CFD applications unless the fuel is treated using a smaller surrogate mixture.

2.2. Continuous thermodynamic model (CTM)

CTMs characterize a multicomponent mixture as a continuous function of a distribution variable to reduce the computational cost compared to full discrete models. The distribution variable, *I*, is usually chosen to be the normal boiling temperature, T_{nb} [29], or molecular weight, *MW* [30], since those properties are relevant to phase change and correlate well with other thermophysical properties.

To convert the DCM described in the previous section to continuous form, the average liquid mole fraction is taken to be a continuous function of the distribution variable, *I*, [31] giving the continuous form of Eq. (1)

(11)

$$\frac{d\bar{x}_l(I)}{dt} = S(I,t)$$

where the source term for the finite diffusivity model is given by

(12)

$$S(I,t) = \left(\frac{15 D_l}{R^2} + \frac{3}{R}\frac{dR}{dt}\right)\left(x_{l,s}(I) - \bar{x}_l(I)\right)$$

The corresponding algebraic expression for $x_{l,s}(I)$ given in Eq. (2) is similarly converted to continuous form:

(13)

$$x_{l,s}(I) = \frac{5 C_l D_l \bar{x}_l(I) + \frac{C_g D_g Sh_g^* ln(1+B_M)}{2B_M} x_{g,\infty}(I)}{5 C_l D_l + C_l R \frac{dR}{dt}\left(1 - \frac{\phi_{l,s}(I)}{\phi_{g,s}(I)}\right) + \frac{C_g D_g Sh_g^* ln(1+B_M)}{2B_M}\frac{\phi_{l,s}(I)}{\phi_{g,s}(I)}}$$

The vapor–liquid equilibrium condition and all other equations and properties required by the model are similarly converted to continuous form (see Section 2.2.2).

CTMs based on pre-determined distributions, like gamma functions [30], [32], have been employed in droplet vaporization models, including those incorporated in CFD codes [33]. While these distribution functions might, in some cases, be adequate to represent the composition of a multicomponent fuel prior to significant vaporization, the distribution becomes distorted throughout the vaporization and/or condensation process, rendering CTMs based on pre-determined distributions lacking.

2.2.1. CA-DQMoM

In contrast to predetermined distributions, quadrature-based moment methods efficiently solve for an evolving continuous distribution without assuming any functional form [31], [34]. For instance, the quadrature method of moments (QMoM) represents the evolution of a continuous distribution by solving for the first 2*N* moments of the distribution, where *N* is the number of nodes used to represent the distribution [34]. The direct quadrature method of moments (DQMoM) solves directly for the *N* nodes (abscissas, or *I*-values) and *N* weights (mole fractions) of an evolving equivalent distribution, which is mathematically identical to QMoM, but can be numerically superior [31]. In the context of droplet vaporization, CA-DQMoM extends DQMoM to account for finite rates of diffusion within a droplet by solving for the nodes and weights associated with two continuous distributions [13], corresponding to the average and surface liquid mole fractions governed by Eqs. (11), (13).

CA-DQMoM for droplet vaporization has been described previously [13] but is summarized here. A moment transformation is applied to Eq. (11) to generate 2*N* equations for the first 2*N* moments of the distribution, $k = 0\text{:}\, 2N-1$.

(14)

$$\frac{d\bar{m}_l^{\,k}}{dt} = \bar{S}_k = \int_0^\infty S(I) I^k dI$$

where,

(15)

$$\overline{S}_k = \int_0^\infty S(I) I^k dI = \int_0^\infty x_{l,s}(I) f(I) dI - \int_0^\infty \overline{x_l}(I) f(I) dI$$

and $f(I)$ is given by

(16)

$$f(I) = \left(\frac{15 D_l}{R^2} + \frac{3}{R}\frac{dR}{dt}\right) I^k$$

A Gaussian quadrature approximation is applied to the average and surface mole fraction distributions, which each have their own weights and nodes:

(17)

$$\int_0^\infty \bar{x}_l(I) f(I) dI \approx \sum_{j=1}^{N} \bar{w}_j f\left(\bar{I}_j\right)$$

(18)

$$\int_0^\infty x_{l,s}(I) f(I) dI \approx \sum_{j=1}^{N} w_{s,j} f\left(I_{s,j}\right)$$

Rather than solving for the moments of the distribution, CA-DQMoM solves directly for the weights and nodes by writing the distribution function for the differential variable as a sum of *N* delta functions

(19)

$$\bar{x}_l(I) = \sum_{j=1}^{N} \bar{w}_j \delta\left(I - \bar{I}_j\right)$$

Differentiating and inserting in Eq. (11) yields

(20)

$$\sum_{j=1}^{N} \frac{d}{dt}\left[\bar{w}_j \delta\left(I - \bar{I}_j\right)\right] = S(I,t)$$

Applying derivative rules, multiplying by I^k, integrating over the distribution and applying rules for integrals of delta functions and their derivatives, one arrives at *2N* equations that can be written in matrix form [31]:

(21)

$$\begin{bmatrix} 1 & \cdots & 1 & 0 & \cdots & 0 \\ 0 & \cdots & 0 & 1 & \cdots & 1 \\ -\bar{I}_1^2 & \cdots & -\bar{I}_N^2 & 2\bar{I}_1 & \cdots & 2\bar{I}_N \\ \vdots & \vdots & \vdots & \vdots & \vdots & \vdots \\ 2(1-N)\bar{I}_1^{2N-1} & \cdots & 2(1-N)\bar{I}_N^{2N-1} & (2N-1)\bar{I}_1^{2N-2} & \cdots & (2N-1)\bar{I}_N^{2N-2} \end{bmatrix} \times \begin{bmatrix} d\bar{w}_1/dt \\ \vdots \\ d\bar{w}_N/dt \\ d(\bar{w}_1\bar{I}_1)/dt \\ \vdots \\ d(\bar{w}_N\bar{I}_N)/dt \end{bmatrix} = \begin{bmatrix} \bar{S}_0 \\ \vdots \\ \vdots \\ \vdots \\ \vdots \\ \bar{S}_{2N-1} \end{bmatrix}$$

The Gaussian quadrature approximations (Eqs. (17), (18)) are substituted in Eq. (15) to obtain the source terms, $\bar{S}_k$, in terms of the weights and nodes.

(22)

$$\bar{S}_k = \left(\frac{15D_l}{R^2} + \frac{3}{R}\frac{dR}{dt}\right)\left[\sum_{j=1}^{N} w_{s,j} I_{s,j}^k - \sum_{j=1}^{N} \bar{w}_j \bar{I}_j^k\right]$$

To solve for the algebraic variables $w_{s,j}$ and $I_{s,j}$, a moment transformation is performed on Eq. (13) and quadrature approximations (17), (18) as well as a corresponding quadrature for the gas-phase boundary,

(23)

$$\int_0^\infty x_{g,\infty}(I) f(I) dI \approx \sum_{i=1}^{n} x_{g,\infty}^i f\left(I_i^i\right)$$

are used. In a CFD context, the *n* discrete species in Eq. (23) would be supplied by the Eulerian-phase solver. Applying the three quadrature approximations to Eq. (13) results in the *2N* coupled algebraic expressions for the surface weights and nodes, given by

$$\sum_{j=1}^{N}\left[5C_lD_l + C_lR\frac{dR}{dt}\left(1-\frac{\phi_{l,s}(I_{s,j})}{\phi_{g,s}(I_{s,j})}\right)+\frac{C_gD_gSh_g^*ln(1+B_M)}{2B_M}\frac{\phi_{l,s}(I_{s,j})}{\phi_{g,s}(I_{s,j})}\right]w_{s,j}I_{s,j}^k$$

(24)

$$=\sum_{j=1}^{N}\quad 5C_lD_l\bar{w}_j\bar{I}_j^k+\sum_{i=1}^{n}\quad\frac{C_gD_gSh_g^*ln(1+B_M)}{2B_M}x_{g,\infty}^i I_i^k$$

Details of the derivation are available elsewhere [13], [20].

2.2.2. Property evaluation for CA-DQMoM

As a type of continuous thermodynamic model, all thermophysical and transport properties required by CA-DQMoM must be interpolated as a function of the distribution variable, *I*, (in addition to being functions of other properties, such as temperature). For instance, in previous implementations, where *I* was taken to be the normal boiling point, T_{nb} [12], [19], the liquid specific heat capacity is given by a linear correlation of $c_{p,I}$ as a function of *I*,

(25)

$$c_{p,l}(\bar{T}_l,I)=\left(C_1+C_2\bar{T}_l\right)+\left(C_3+C_4\bar{T}_l\right)I$$

Properties of the mixture are then obtained by continuous forms of mixing rules. If the mixing rule is linear, weighting the property by the liquid mole fraction and integrating over the entire distribution yields a mixture property in terms of *k* moments of the liquid mole fraction distribution, m_l^k. For instance, for the liquid specific heat capacity, this would yield

(26a)

$$c_{p,l}(\bar{T}_l)=\int_0^\infty x_l(I)\,c_{p,l}(\bar{T}_l,I)dI$$

(26b)

$$c_{p,l}(\bar{T}_l)=\left(C_1+C_2\bar{T}_l\right)\int_0^\infty x_l(I)\,dI+\left(C_3+C_4\bar{T}_l\right)\int_0^\infty x_l(I)\,IdI$$

(26c)

$$c_{p,l}(\bar{T}_l)=\left(C_1+C_2\bar{T}_l\right)m_l^0+\left(C_3+C_4\bar{T}_l\right)m_l^1$$

Some mixture properties are defined for the bulk liquid or vapor, some are defined at the interface, and some properties characteristic of the vaporization (or condensation) flux are “flux-weighted” rather than weighted by the mole fraction of a phase/location. Following a procedure similar to Eq. (26), it can be shown [26] that flux-weighted mixture quantities are given in terms of moments of the flux fractions, m_ς^k. These flux moments are

expressed in terms of the moments on the vapor side of the interface, $m_{g,s}^k$, the moments at the far-field boundary, $m_{g,\infty}^k$, and the Spalding mass transfer number, B_M, by:

(27)

$$m_\zeta^k = \frac{B_M + 1}{B_M} m_{g,s}^k - \frac{1}{B_M} m_{g,\infty}^k$$

2.2.3. Optimized distribution variable

The central insight of this paper is that CTMs, including CA-DQMoM, can be used to directly predict the vaporization (condensation) flux of chemical functional groups from (to) a multicomponent fuel droplet by tailoring the distribution variable, *I*. This obviates the need for the delumping model and enables application of the hybrid approach to physical models that may be necessary for high-pressure environments. Because CTMs require that all properties be correlated as functions of the distribution variable, direct prediction of functional group fluxes implies that these functional groups must be well-correlated by the distribution variable. Because mixing rules yield expressions involving the moments of the distribution, it is advantageous that these correlations be polynomial. This is because quadrature methods solve for a certain number of moments of the evolving species distribution, and the moments appear in the equations for the properties of the mixture, as illustrated in Eq. (26c).

While T_{nb} and *MW* are often used as distribution variables for CTMs [29], [30], neither can satisfactorily correlate the important chemical functional groups that govern the chemical behavior of multicomponent hydrocarbon fuels. This is illustrated in Fig. 2, which shows the dependence of the chemical functional groups on the normal boiling temperature, T_{nb}, for the species comprising Jet-A (discussed in Section 3.2). Although it might be possible to employ a separate distribution for every chemical family (e.g. n-alkanes, *iso*-alkanes) to partially address this issue, this approach has been found to be impractical due to computational cost and numerical instability.

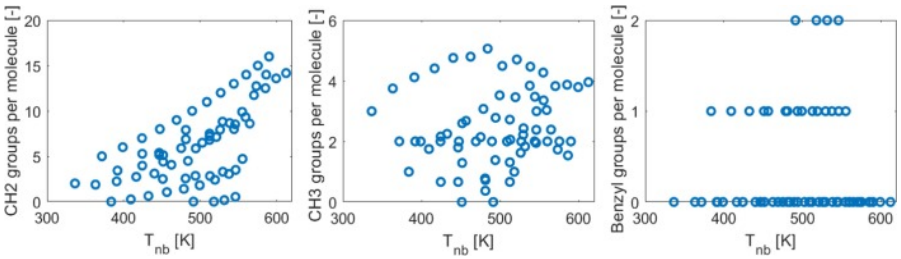

Fig. 2. Dependence of the ratios of (a) CH_2, (b) CH_3 and (c) benzyl-type functional groups per molecule on the normal boiling temperature, for Jet-A.

Therefore, to directly calculate the flux of chemical functional groups in addition to thermophysical and transport properties, a new, strictly mathematical (without physical significance) distribution variable, known simply as *I,* can be developed using optimization. The purpose of the optimization routine is to assign to every hydrocarbon species a value of *I* such that the dependence of thermophysical properties, transport properties and the number of CH_3, CH_2 and benzyl- groups per molecule (y_{CH3}, y_{CH2}, y_{benzyl}) on *I* is approximately polynomial. The values for the thermophysical and transport properties at various temperatures are obtained from Yaws [27], and the functional groups associated with each species are based on a simple average of all isomers of that species in the appropriate chemical family in the NIST database (this is discussed in Section 3.2).

The optimization procedure employed a genetic algorithm to determine *I*-values for every discrete species such that an objective function involving residuals of polynomial fits of the desired thermophysical properties and

functional group to the distribution variable, *I,* was minimized. A single-objective genetic algorithm was employed, although multi-objective optimization could be pursued in the future. The objective function was chosen to be

(28)

$$F = F_{space}[(1 - R^2_{P-Ra}) + (1 - R^2_{CH3})^{0.8} + (1 - R^2_{CH2})][(1 - R^2_{P-Ra}) + (1 - R^2_{CH3}) + (1 - R^2_{CH2})]$$

The first term ensures proper spacing between *I* and values and prevents clustering. The remaining terms contain coefficients of determination (R^2 values) for polynomial fits between three important properties and the distribution variable, *I*. The three properties include those influencing vaporization (the Peng-Robinson *a* parameter), the functional group distributions (y_{CH3}, y_{CH2}) and properties associated with the size of the molecule (y_{CH2}, *a*), which tends to correlate with other properties not explicitly included in the objective function. Constraints were also used to force the benzyl-group distribution to be a double step-function with *I,* because all fuel components had either zero, one or two benzyl-group per molecule. While this objective function was determined in an ad-hoc manner, it serves as proof-of-concept for the idea of using tailored distribution functions in CTMs.

This optimization procedure constitutes a pre-processing step that only needs to be performed once for a given fuel. This is akin to the process of optimizing the composition of a physical–chemical surrogate. Furthermore, the optimized *I*-distribution obtained for one fuel can serve as the basis for others, since many hydrocarbon fuels (e.g. jet fuels like Jet-A, JP-8) contain similar sets of major species [35].

Even though the objective function involved just a few properties/functional groups, all properties required by the hybrid droplet model were subsequently fit to the optimized *I*-distribution to generate polynomial correlations for use in the hybrid droplet vaporization model. Most polynomials were third order in *I*. Results for selected properties and functional groups are shown in Fig. 3. It is noted that the Peng-Robinson *a* parameter is fit as $a^{1/2}$, as is done when using *MW* as the distribution variable [36]. The quality of the fits for the thermophysical and transport properties are comparable to those obtained using the typical distribution variable (T_{nb}) previously, but the current approach has the advantage that it enables CA-DQMoM to directly predict the vaporization or condensation flux of key functional groups . A second advantage of the present approach is its improved ability to incorporate species from different chemical families in a single distribution.

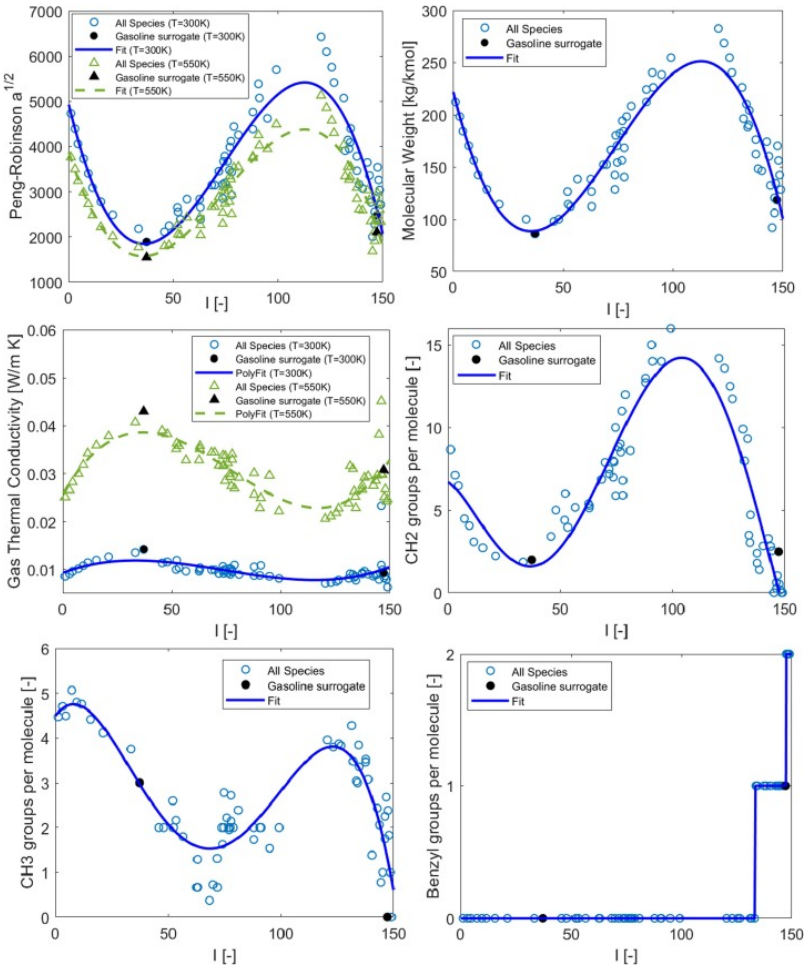

Fig. 3. Selected correlations of properties and functional groups with the optimized distribution variable, *I*. (a) Peng-Robinson parameter, $a^{1/2}$, at two temperatures (b) molecular weight, *MW*, (c) gas-phase thermal conductivity, k_g, at two temperatures, and (d)-(f) the ratios of CH_2, CH_3 and benzyl-type functional groups per molecule, respectively. "All species" refers to those comprising the target fuel, discussed in Section 3.2, and the "gasoline surrogate" is two more species relevant to the third test case presented in Section 3.4.

2.3. Functional group matching and adaptive surrogate formulation

Functional group matching has been described previously [12]. FGM takes as input the fluxes of key functional groups from the droplet, and uses it to construct a time-dependent, chemical surrogate composed of a few discrete species, with the same distribution of functional groups [12], as shown in Fig. 1. FGM was inspired by the finding of Won et al. which demonstrated a link between combustion property targets (CPTs) and chemical functional groups (CH_2, $(CH_2)_n$, CH_3, CH, C, and Benzyl-type) [5]. The FGM method uses four coupled algebraic equations to match the molar flow rates of benzyl-type functional groups, the sum of CH_2 and $(CH_2)_n$ functional groups, CH_3 functional groups and the molecular weight of the vaporization/condensation flux to those same quantities in the instantaneous flux of the discrete chemical surrogate. In a CFD context, the instantaneous flux of these species would serve as the species source terms for the Eulerian phase. The four species employed for the chemical surrogate are the same as in [12] and are shown in Table 1. Except for n-heptane, these four species are the same as the chemical surrogate employed by Won et al. [5] for Jet-A. The chemical surrogate species can be easily changed to meet the needs of gas-phase chemical kinetic models.

Table 1. Chemical surrogate components and their functional groups.

Class	**Species**	**Formula**	**CH_2**	**$(CH_2)_n$**	**CH_3**	**CH**	**C**	**Benzyl**

n-alkane	n-heptane	C7H16	0	5	2	0	0	0
n-alkane	n-hexadecane	C16H34	0	14	2	0	0	0
iso-alkane	*iso*-dodecane	C12H26	2	0	7	1	2	0
aromatic	1,3,5-trimethylbenzene	C9H12	0	0	3	0	0	1

The original hybrid model performs a delumping step prior to functional group matching (see Fig. 1), to recover the mole fractions and fluxes of all discrete species from the droplet. Delumping is based on the fact that many droplet models appropriate for incorporation in CFD codes are nonlinear, but the nonlinearity is associated solely with terms representative of the multicomponent mixture as a whole [19]. Therefore, the results of the CTM can be inserted for the nonlinear terms in the governing differential equation for $\bar{x}_l^i$, thus linearizing the equations. The first order, linear ordinary differential equations (ODEs) can then be solved analytically and efficiently using the integrating factor method.

Whereas the original hybrid method used the delumped (discrete) fluxes as input to FGM, the proposed hybrid method with the optimized distribution variable uses CA-DQMoM to directly calculate the functional group distribution and molecular weight of the vaporization flux.

2.4. Combustion property calculations

To assess the ability of the hybrid model to predict the impacts of preferential vaporization on combustion behavior, the instantaneous CPTs for the vaporization flux can be evaluated. The CPTs most relevant to global combustion behavior for jet fuels are molecular weight (MW), hydrogen to carbon ratio (H/C), derived cetane number (DCN), and threshold sooting index (TSI) [5]. The MW and H/C ratio of the full target fuels are calculated with linear blending rules and the DCN is calculated using the regression developed by Won et al. [5]. The TSI cannot be calculated for the full DCM because of a lack of experimental data and is therefore not considered when comparing the performance of the hybrid models and the physical–chemical surrogate. It is also noted that the CPTs would not be calculated by the hybrid model when implemented in a CFD context and are evaluted here for assessment purposes only.

2.5. Numerical approach

The hybrid models and the DCMs were integrated in time using the IDA solver developed by the Lawrence Livermore National Laboratory. Both CA-DQMoM and the DCM require an ordinary differential equation for the evolution of droplet radius, R, and average liquid temperature, $\bar{T}_l$, as well as an algebraic equation for $T_{l,s}$. With the Peng-Robinson equation of state, CA-DQMoM requires 2N differential equations (for the average weights and nodes, $\bar{w}_j$ and $\bar{I}_j$) and 3N algebraic equations (for the weights and nodes at the liquid surface, $w_{s,j}$ and $I_{s,j}$, and for the gas weights at the interface, $w_{sg,j}$), where N is the number of nodes used in CA-DQMoM. The number of nodes, N is typically between two and four. In the test cases presented in Section 3.4, the number of nodes, N = 4. The DCM requires n differential equation (for $\bar{x}_l^i$) and 2n algebraic equations (for $x_{l,s}^i$ and $x_{g,s}^i$). For the full target fuel, n = 67 (see Section 3.2), while for the physical–chemical surrogate, n = 9 (see Section 3.3).

3. Results and discussion

3.1. Validation of physical model for droplet vaporization

Although the hybrid approach can be applied to a variety of droplet vaporization models with different levels of complexity, the fidelity of the physical model outlined in Section 2.1 is first evaluated by comparing predictions of the DCM to existing experimental data. Comparisons to multicomponent, ambient pressure data and to single-component, elevated pressure data will be presented.

Runge et al. [37] measured the evolution of 639 µm diameter droplets of JP-8 at ambient temperature (294 K) and pressure (1 bar) with a relative velocity of 3 m/s. To account for the convective conditions, the Sherwood and Nusselt number correlations given by Abramzon and Sirignano [23] are employed to determine Sh_g^* and Nu_g^* and the corresponding film radius, R_f. The JP-8 composition used in the full DCM is based on Edwards' data which consists of 67 species, mostly specified by carbon number and chemical family [38]. The composition for the JP-8 droplet employed in the DCM is the same as the 67 species employed by Govindaraju and Ihme [39] based on Edwards' data.

Fig. 4 compares the predictions of the full DCM to the measurements of Runge et al. [37]. DCM predictions for *d*^2 match the experimental data well. In addition to validating the physical model described in Section 2.1, this comparison provides confidence in the adequacy of experimental multicomponent fuel characterizations provided in terms of carbon number and chemical family to represent complex hydrocarbon fuels. This point is discussed further in Section 3.2.

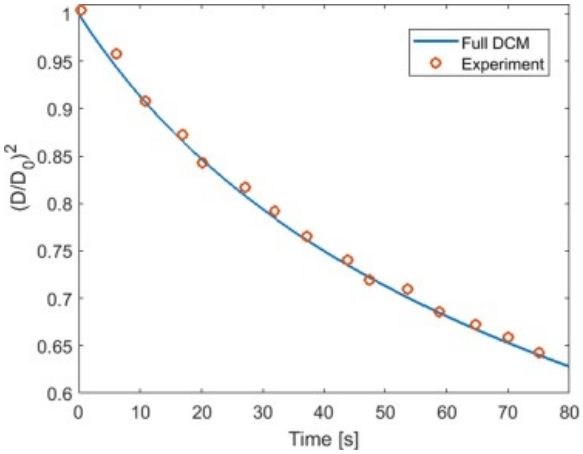

Fig. 4. Comparison of the squared diameter variation predicted by the physical model (DCM) with experimental data, for a multicomponent droplet (JP-8) at ambient pressure [37].

Nomura et al. [40] measured the variation of droplet diameter for suspended n-heptane droplets at pressures of 0.1–5 MPa, under quiescent, microgravity conditions. Fig. 5 shows a comparison between DCM predictions and the data of Nomura et al. for pressures up to 1 MPa. The agreement is adequate, but at increasing pressures the deviation between experiment and prediction increases. This is not unexpected, since the physical model employed in this paper does not incorporate gas solubility, pressure-dependent property correlations, droplet non-sphericity [41] and vapor-phase transience [42]. Another source of disagreement is likely the uncertainty associated with convection and transience in the first 0.16 s of the experiment [40], during which the experimental droplet traversed the hot chamber on its way to the test position and experienced convective heat up, reducing the measured vaporization time [43]. While future work will focus on incorporating high-pressure effects, the comparisons with the experimental data of Runge and Nomura demonstrate that the physical model is adequate for comparing the hybrid approach to the physical–chemical surrogate approach for multicomponent hydrocarbon droplets.

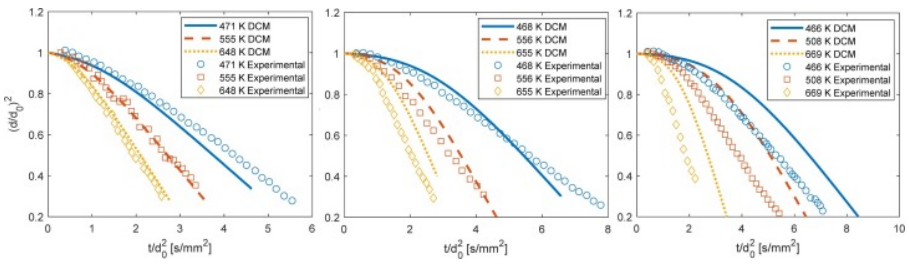

Fig 5. Comparison of the squared diameter variation predicted by the physical model (DCM) with experimental data [40] for heptane at (a) 0.1 MPa, (b) 0.5 MPa and (c) 1 MPa.

3.2. Target fuel for test cases

The test cases in Section 3.4 are based on droplets of Jet-A fuel. The characterization of the fuel is based on Edwards' summary for Jet-A (POSF-10325) in which most species are specified by carbon number and chemical family [38], which is in turn based on the measurements of [44]. The corresponding composition for the target fuel is the same 67 species employed by Govindaraju and Ihme (see supplemental material therein) [39]. The CPTs and advanced distillation curve for this target fuel are compared to experimental data for Jet-A (POSF 10325) in this section.

Fig. 6 shows a comparison between the experimentally measured [35] advanced distillation curve for Jet-A (POSF 10325) and the calculated advanced distillation curve for the 67-component target fuel. The advanced distillation curve is a better representation of the thermodynamic states of a multicomponent mixture than the ASTM D86 distillation curve [45], so the experimental data in Fig. 6 for Jet-A is taken from a source employing the advanced distillation curve methodology [35]. The calculation of the advanced distillation curve for the 67-component target fuel shown in Fig. 6 is performed following the procedure outlined by Kim et al. [46], by determining the temperature of the bubble point at each fraction of distilled volume using a nonlinear solver routine and subsequently solving for the composition of the remaining liquid. Good agreement between the experimentally measured advanced distillation curve for Jet-A (POSF 10325) and the calculated advanced distillation curve for the target fuel is observed.

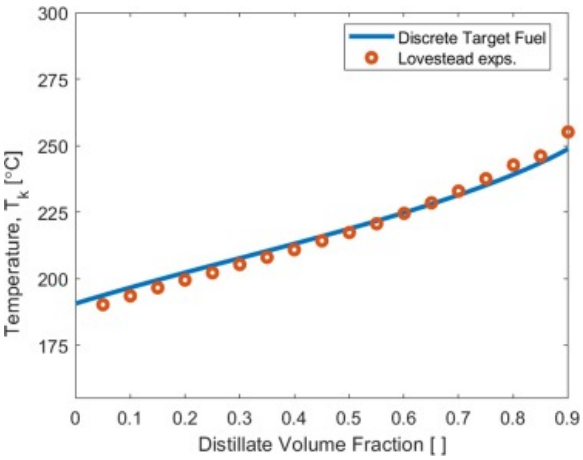

Fig. 6. Comparison between advanced distillation curve measured for Jet A-10325 [35] and the calculated advanced distillation curve for the 67-component target fuel used to represent Jet A-10325.

Although the precise composition of all isomers is not known experimentally, this does not introduce undue uncertainty into the droplet vaporization behavior. To demonstrate this, the droplet vaporization/condensation behavior calculated using the full DCM for the target fuel [39] is compared to that for a fuel in which the 67 species are treated as being composed of a simple average of every isomer of that chemical family and formula found in the Yaws database (a total of 1079 species) [27]. It is observed in Fig. 7 that the droplet vaporization behavior, as characterized by the instantaneous vaporization rate, is not strongly affected by the precise composition. This suggests that experimental data such as that measured by Lovestead et al. [35] and Striebich et al. [44] is adequate for representing the droplet vaporization behavior of the target fuel and can be used as a basis for model development.

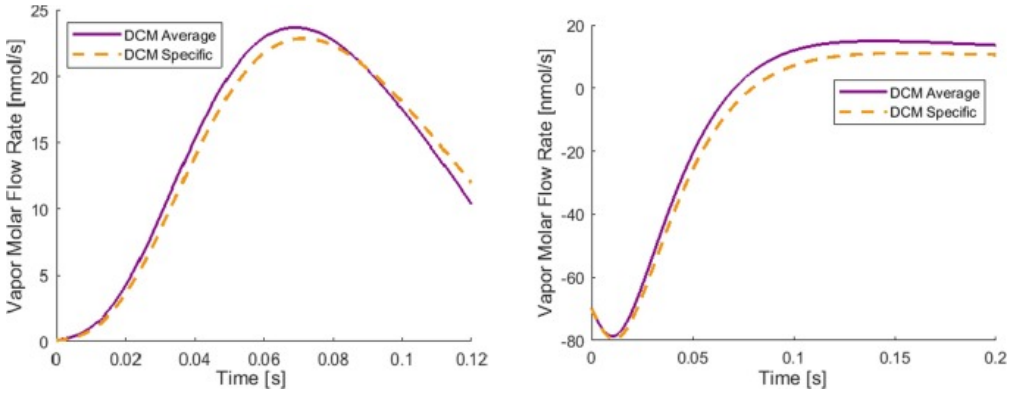

Fig. 7. Comparison of target fuels with properties composed of average of all isomers in the Yaws database [27] and composed of specific isomers [39], for vaporization in (a) pure air and (b) fuel-rich conditions.

Even though the exact isomeric composition does not significantly alter the target fuel's vaporization/condensation behavior, it can certainly affect the resultant chemistry and combustion properties of the gas phase via its impact on functional group distributions. Because the fuel's functional group distribution correlates with measurable combustion property targets [5] and can even be determined directly by NMR [8], the specific isomeric composition of the target fuel could be tuned to match that of the experimental fuel and its combustion property targets, if necessary. In the present test case, no tuning was used and the functional group distribution associated with each of the 67 species in the DCM were calculated using an average of all hydrocarbon species of that family and chemical formula in the NIST database.

The CPTs (molecular weight, DCN, and H/C ratio) of this target fuel were calculated and are shown in Table 2, in which they are compared to the measured CPTs for POSF-10325 summarized by Edwards [38]. It is noted, that in Table 2, DCN is calculated using the new quantitative structure–property relation (QSPR) regression developed by [8] that accounts for cycloalkane functionality, since that functionality is, of course, present for the experimentally measured fuel. It is seen in Table 2 that the CPTs (and hence the functional group distribution [5]) of the target fuel used to represent POSF-10325 agree closely with the experimental values.

Table 2. Comparison between experimentally measured CPTs for Jet A-10325 and the CPTs for the 67-component target fuel used to represent Jet A-10325.

CPT	**POSF-10325 [38]**	**Target Fuel**
Molecular Weight	159.0	158.4
H/C Ratio	1.91	1.94
DCN	48.3	47.9*

*DCN of the target fuel is calculated from QSPR regression [8] that accounts for cycloalkane functionality.

Because the CPTs and distillation curve for the 67-component target fuel match those measured experimentally, and because the droplet vaporization process and physical properties do not appear to be significantly affected by the isomeric composition, it is concluded that the present target fuel representation of Jet-A is acceptable. Nonetheless, it is noted that emerging techniques using two-dimensional gas chromatography with time-of-flight mass spectrometry have the potential to quantify the detailed composition of hydrocarbon fuels with even higher levels of precision [47].

3.3. Physical-chemical surrogate formulation

To compare the performance of the hybrid droplet vaporization-adaptive surrogate approach to the physical–chemical surrogate approach, a physical–chemical surrogate for the present target fuel was formulated following the procedure outlined by Won et al. [5]. An optimization routine was used to determine the mole

fractions of the nine-component physical–chemical surrogate in [5] to match the CPTs, as well as the advanced distillation curve, of the target fuel (described in Section 3.2). The resultant composition of the physical–chemical surrogate is shown in Table 3. It is noted, that in formulating the physical–chemical surrogate, the impact of the cycloalkane functionality on DCN was omitted, as in [5], because the chemical surrogate used in the functional group matching does not include a cycloalkane species (Table 1). This could be included in the future, but it does not affect the comparison between the hybrid approach and physical–chemical surrogate approach presented in Section 3.4.

Table 3. Composition of the physical–chemical surrogate used to represent the target fuel.

Component	**Surrogate Mole Fraction**
n-octane	0.0003
n-decane	0.0003
n-dodecane	0.3009
n-tetradecane	0.2365
n-hexadecane	0.0330
iso-octane	0.0150
iso-dodecane	0.0475
1,3,5-trimethylbenzne	0.3652
toluene	0.0014

The calculated advanced distillation curves for the physical–chemical surrogate (Table 3) and for the full target fuel are shown in Fig. 8. The advanced distillation curves for the target fuel and the physical–chemical surrogate are both calculated as described in Section 3.2 [46]. It is observed that the distillation curve of the physical–chemical surrogate closely matches that of the target fuel.

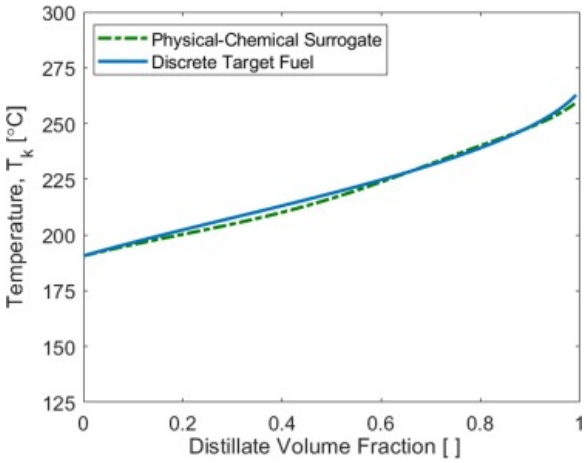

Fig. 8. Comparison between the advanced distillation curves calculated for the physical–chemical surrogate and its corresponding target fuel.

The calculated CPTs for the physical–chemical surrogate (Table 3) and the full target fuel are shown in Table 4. Good agreement between the physical–chemical surrogate and the target fuel is obtained for all three CPTs. Because the CPTs and the advanced distillation curve of the physical–chemical surrogate match those of the full target fuel, this nine-component physical–chemical surrogate represents the state-of-the-art approach for modeling vaporization of multicomponent fuel droplets, and will be compared to the hybrid droplet vaporization-adaptive surrogate model proposed in this paper.

Table 4. CPTs calculated for the physical–chemical surrogate and its corresponding target fuel.

CPT	Physical-Chemical Surrogate	Target Fuel
Molecular Weight	159.5	158.4
H/C Ratio	1.92	1.94
DCN	55.3*	54.9*

*DCN for both fuels is calculated from QSPR regression [5] that does not account for cycloalkane functionality, as explained in the text.

3.4. Comparison of hybrid models to physical–chemical surrogate and full DCM

Droplet vaporization behavior for the full discrete target fuel (DCM) will be compared to three models which approximate it: the hybrid model with the optimized distribution, the hybrid model with delumping, and the physical–chemical surrogate model formulated to match the target fuel.

3.4.1. Test case 1: vaporization in pure air

For vaporization of a 100 µm droplet into pure air at 600 K and 1 MPa, the evolution of the instantaneous total molar flux is shown in Fig. 9. Comparing the droplet vaporization behavior predicted by the two versions of the hybrid model to that calculated using the full DCM, it is observed that CA-DQMoM, using either normal boiling point (“Hybrid Delumping”) or the optimized distribution variable (“Hybrid Direct”), can successfully reproduce the vaporization behavior of a multicomponent droplet. The nine-component physical–chemical surrogate ("Surrogate") also replicates the droplet vaporization behavior for these conditions, although the accuracy is lower than the continuous thermodynamic models.

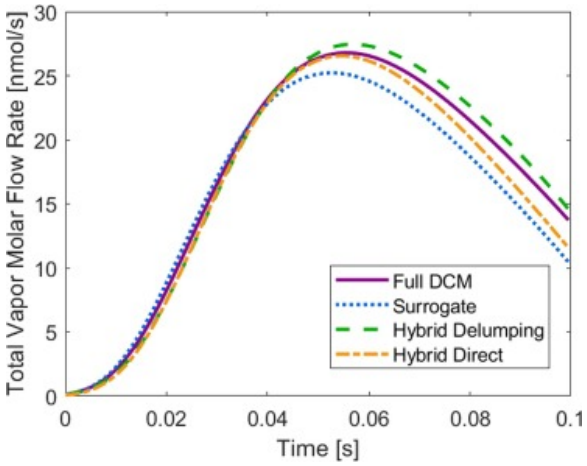

Fig. 9. Evolution of the total molar flow rate for vaporization in air, calculated using the full DCM for the target fuel, the physical–chemical surrogate, CA-DQMoM with delumping and CA-DQMoM with direct prediction of functional groups.

Fig. 10 shows the instantaneous flux of the key chemical functional groups for the full target fuel DCM and the three models that approximate it. The hybrid delumping method reproduces the functional group fluxes with the highest accuracy, followed by the hybrid direct method (which uses the optimized distribution variable) which is less accurate in its prediction of CH_3. Both hybrid methods are more accurate in predicting the flux of chemical functional groups than the physical–chemical surrogate approach and the difference is especially pronounced for the benzyl-group.

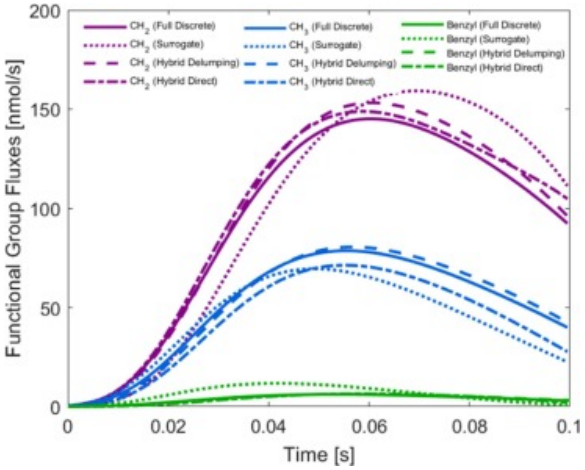

Fig. 10. Flux of chemical functional groups for vaporization in air, calculated using the full DCM for the target fuel, the physical–chemical surrogate, CA-DQMoM with delumping and CA-DQMoM with direct prediction of functional groups.

The hybrid models use a CTM (CA-DQMoM) to predict the vaporization/condensation/physical behavior of the droplets and then use the functional group matching model to generate a small chemical surrogate source term for the Eulerian phase of CFD codes [12]. Although not the focus of this paper, the mole fractions of the chemical surrogate flux calculated by FGM for the hybrid direct model are shown in Fig. 11. The fraction of the heavier n-alkane and 1,3,5-trimethylbenzene increase at later times as the less volatile species begin to vaporize, while the lighter n-alkane becomes less prevalent in the chemical surrogate. The adaptive nature of the chemical surrogate composition enables CFD codes to better capture the impacts of preferential vaporization on gas-phase chemistry at a lower computational cost than the physical–chemical surrogate approach, due to its smaller size. As noted, the species comprising the chemical surrogate can be easily altered.

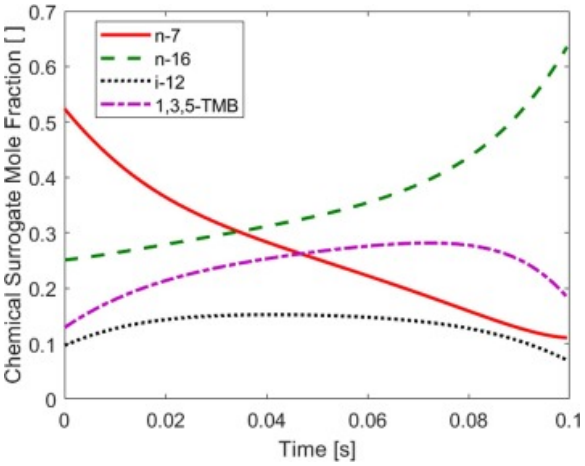

Fig. 11. Instantaneous composition of the adaptive chemical surrogate calculated with the direct hybrid method for vaporization in pure air.

Using the instantaneous composition of the adaptive chemical surrogate flux, the instantaneous combustion property targets of the flux are calculated for the hybrid models and compared to the physical–chemical surrogate and to the full DCM in Fig. 12, for times at which the total vaporization rate is greater than 10 nmol/s. The hybrid model with delumping captures these properties most accurately, followed by the hybrid direct model with the optimized distribution variable. Matching the evolution of the chemical functional groups (Fig. 10) is key to matching the distillation-resolved combustion behavior [5], so it is not surprising that the relative

performance of the three approximate models is the same in Fig. 10, Fig. 12. While the physical–chemical surrogate matches the molecular weight at early times with more accuracy than the direct hybrid model, the latter produces a better match for the H/C ratio and the DCN throughout vaporization. The impact of preferential vaporization on the Eulerian phase is apparent in the variation of the CPTs of the flux in Fig. 12. It is noted that in a CFD context, the CPTs would not need to be calculated.

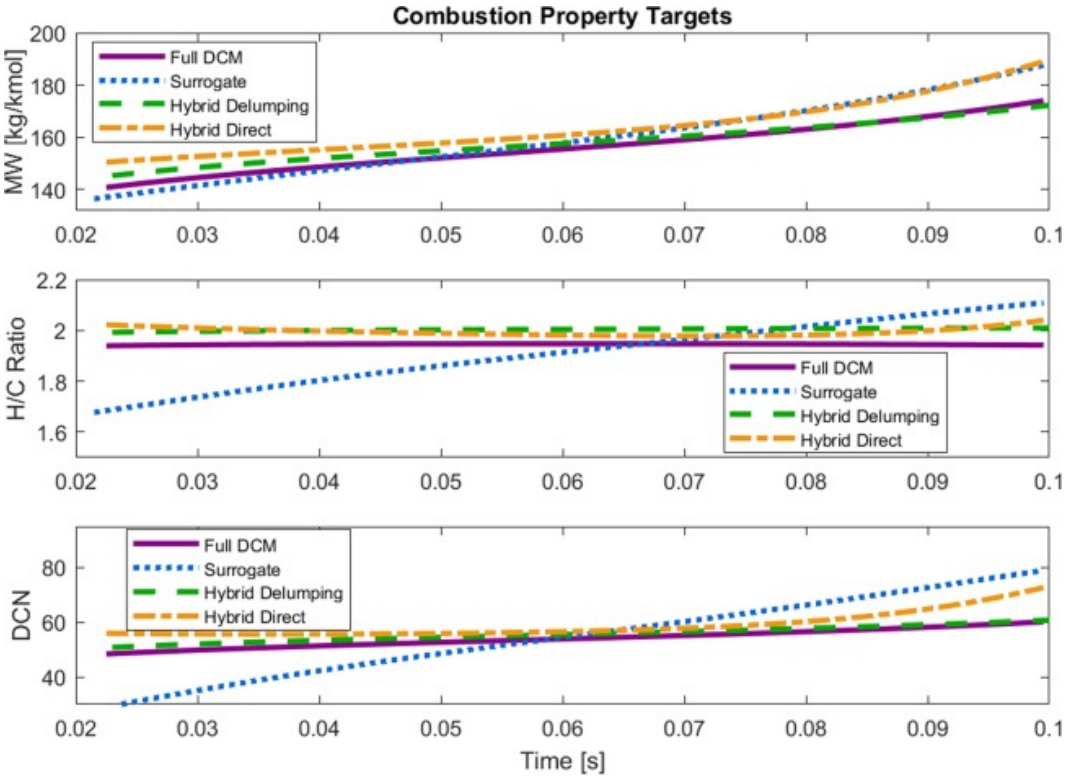

Fig. 12. Chemical properties of the instantaneous flux for vaporization in air, calculated using the full DCM for the target fuel, the physical–chemical surrogate, CA-DQMoM with delumping and CA-DQMoM with direct prediction of functional groups.

Although the physical–chemical surrogate is formulated to match the pre-vaporized CPTs (and therefore the pre-vaporized functional groups) as well as the distillation curve, there is no constraint ensuring that the functional group distribution of the lower (higher) volatility species in the physical–chemical surrogate matches the functional group distribution of the lower (higher) volatility species of the target fuel. With CA-DQMoM, however, the properties governing vaporization (e.g. Peng-Robinson parameters) as well as the functional group distributions are both *correlated with the same optimized distribution variable*. This ensures that the functional group fluxes throughout vaporization match those of the target fuel and is likely the reason that the functional group fluxes are predicted more accurately with the hybrid approach.

3.4.2. Test case 2: vaporization in a fuel-rich mixture

The models were also tested under conditions in which condensation initially dominates vaporization. While, in reality, the fuel species surrounding a droplet would not be constrained to those present in the physical–chemical surrogate, practically, a CFD code would not track more than several transported fuel components in addition to the reaction products and intermediates. However, even in a CFD context, the vapor surrounding a droplet could consist of species other than those comprising the physical–chemical surrogate, either due to gas-phase chemistry or in a dual-fuel combustion environment. There is no obvious way in which the physical–chemical surrogate approach can accommodate species beyond those which comprise the surrogate. Therefore,

a comparison will be performed first for a case in which the droplet boundary conditions only include species comprising the physical–chemical surrogate, and subsequently for a case in which other species are present in the vapor surrounding the droplet (Section 3.4.3).

The evolution of total molar flux is shown in Fig. 13 for a 100 µm droplet injected into an environment at 600 K, 1 MPa and containing 14.3% fuel by mass. The fuel in the vapor phase is comprised of the more volatile species present in the physical–chemical surrogate: 0.01 mole fraction of n-octane, *iso*-octane, n-decane and toluene. The initial negative molar flux indicates condensation occurs at early times, after which the droplet heats up and vaporization dominates.

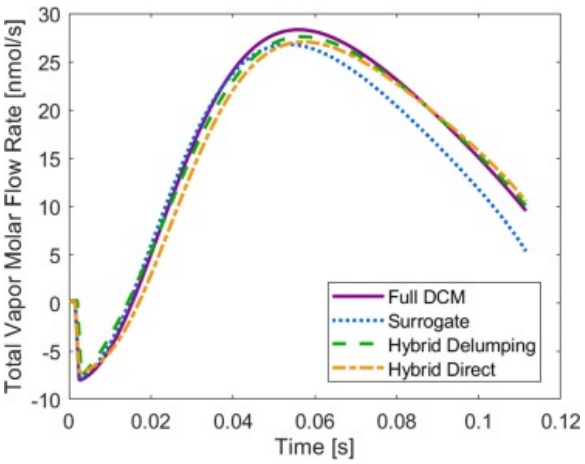

Fig. 13. Evolution of the total molar flow rate during the vaporization into a fuel-rich mixture, calculated using the full DCM for the target fuel, the physical–chemical surrogate, CA-DQMoM with delumping and CA-DQMoM with the new distribution variable.

The hybrid method with delumping is again the most accurate of the three methods for representing the droplet vaporization behavior. The hybrid method with the optimized distribution variable (hybrid direct) performs reasonably well when the vaporization fluxes are negative (condensation), however, at early times, the physical–chemical surrogate is more accurate in capturing the droplet behavior. This test case is representative of others that indicate that during condensation and subsequent re-vaporization of species present in the physical–chemical surrogate itself, the physical–chemical surrogate approach is quite accurate in representing the droplet behavior. However, as the droplet heats up and vaporization of the full fuel begins to dominate, both hybrid methods (even the direct hybrid method) become more accurate, as they better represent the full target fuel. This can be observed in the later times in Fig. 13.

The functional group fluxes for the test case with initial condensation are shown in Fig. 14 for the three approximations to the full DCM. The hybrid model with delumping reproduces the instantaneous flux of key functional groups to/from the droplet with the highest accuracy. Despite the accuracy of the physical–chemical surrogate in predicting droplet vaporization at early times (Fig. 13), both hybrid methods are more accurate than the physical–chemical surrogate approach in predicting the distillation-resolved flux of functional groups. This is particularly the case for the flux of CH_2– and benzyl-groups, which is similar to Fig. 10, although to a lesser extent. The CPTs of the vaporization flux are shown in Fig. 15 for times in which the vaporization flux is larger than 10 nmol/s. Despite the accuracy of the physical–chemical surrogate in predicting the droplet vaporization behavior at early times (Fig. 13), it is not very accurate in predicting the instantaneous H/C ratio or DCN, due to its inaccuracy at predicting the distillation-resolved functional group fluxes (Fig. 14). The hybrid model with delumping is the most accurate, and the direct hybrid model has similar accuracy for H/C ratio and DCN, although it is the least accurate in predicting molecular weight.

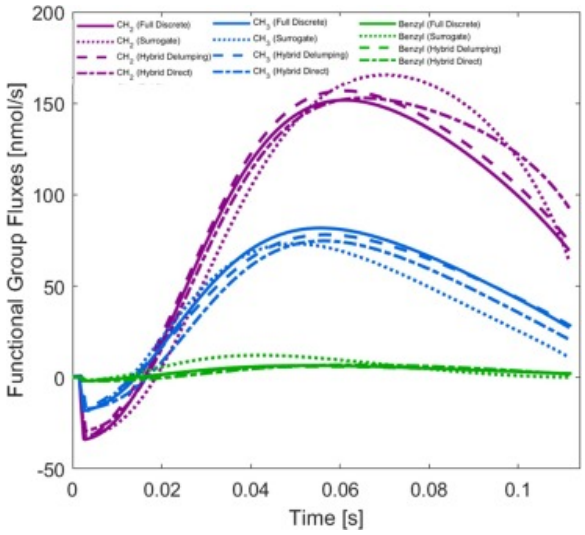

Fig. 14. Flux of chemical functional groups for vaporization into a fuel-rich mixture, calculated using the full DCM for the target fuel, the physical–chemical surrogate, CA-DQMoM with delumping and CA-DQMoM with direct prediction of functional groups.

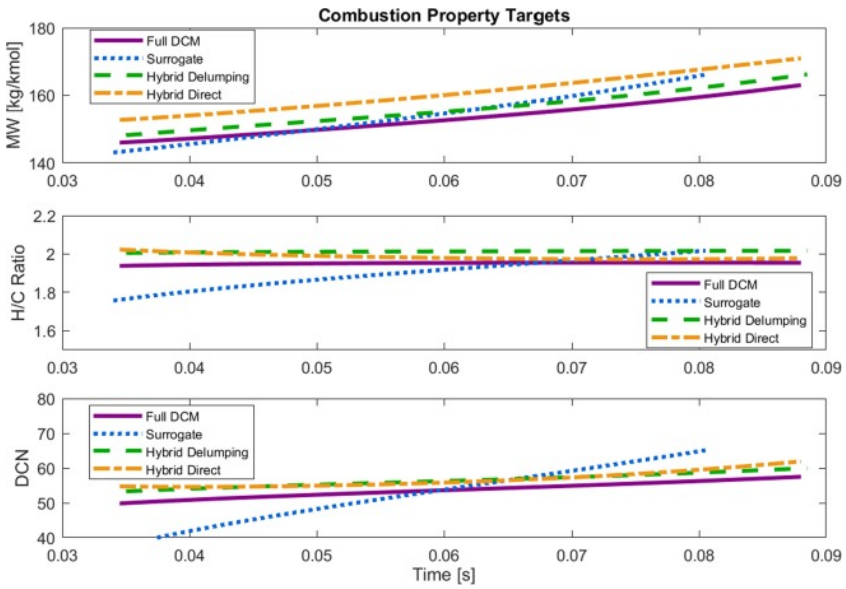

Fig. 15. Chemical properties of the instantaneous flux for vaporization into a fuel rich mixture, calculated using the full DCM for the target fuel, the physical–chemical surrogate, CA-DQMoM with delumping and CA-DQMoM with direct prediction of functional groups.

3.4.3. Test case 3: vaporization in presence of species not comprising physical–chemical surrogate

The final test case compares the performance of the hybrid approaches and the physical–chemical surrogate approach for conditions in which species beyond those present in the physical–chemical surrogate surround the droplet. This situation might arise, for instance, due to pyrolysis chemistry in the gas-phase or in a dual-fuel combustion environment. As an example of the latter, a Direct Dual Fuel Stratification (DDFS) environment [48], in which both the less reactive fuel (gasoline) and the more reactive fuel (Jet-A, in this case) are injected directly, is represented at 600 K and at 1 MPa. At the time when the more reactive fuel is injected, portions of the spray may encounter localized regions rich in gasoline. Consistent with a CFD context, the gasoline vapor surrounding the droplet will be represented by a chemical surrogate, which is comprised of indane and methylpentane [49], with each present at a mole fraction of 0.05.

It is not immediately clear how the physical–chemical surrogate model can best accommodate the presence of species beyond those comprising the surrogate. The two gasoline surrogate species in this test case, indane and methylpentane, were treated as 1,3,5 trimethylbenzne and n-octane, respectively. For the direct hybrid method, the optimized distribution can be explicitly tailored, if needed, to ensure that the gasoline surrogate species' properties are well-correlated with the distribution variable, *I*. The *I*-values for the gasoline surrogate species and its ability to correlate key properties are shown with the filled symbols in Fig. 3, where it is apparent that the optimized CTM can readily incorporate the presence of species not comprising the multicomponent fuel.

For conditions dominated by species not comprising the physical–chemical surrogate, the accuracy of the physical–chemical surrogate approach in predicting droplet behavior decreases when condensation occurs, compared to the previous test case. This can be observed in the early times of Fig. 16. Nonetheless, it still represents the instantaneous droplet vaporization rate reasonably well. For this test case, it is observed that the hybrid model with delumping is less accurate than the direct hybrid model at later times.

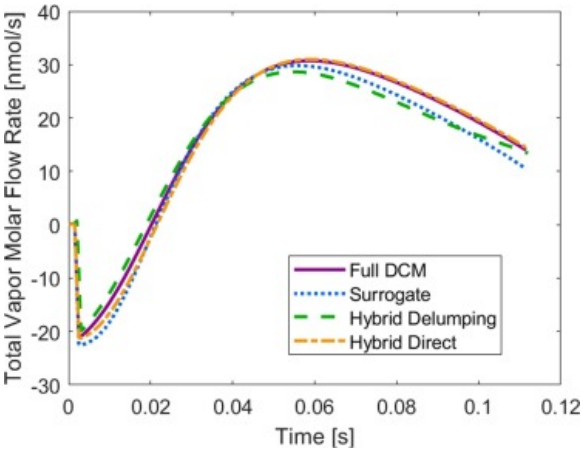

Fig. 16. Evolution of the total molar flow rate during the vaporization into a mixture containing species not present in the physical–chemical surrogate, calculated using the full DCM for the target fuel, the physical–chemical surrogate, CA-DQMoM with delumping and CA-DQMoM with the new distribution variable.

The functional group fluxes and CPTs of the flux are shown in Fig. 17, Fig. 18, respectively. It is observed that the direct hybrid method is the most accurate model at reproducing the DCM data for the functional group fluxes and the CPTs for the DDFS test case, in which non-fuel species surround the droplet. This observation extends to include the molecular weight of the flux, in contrast to the previous test cases, as seen in Fig. 18a.

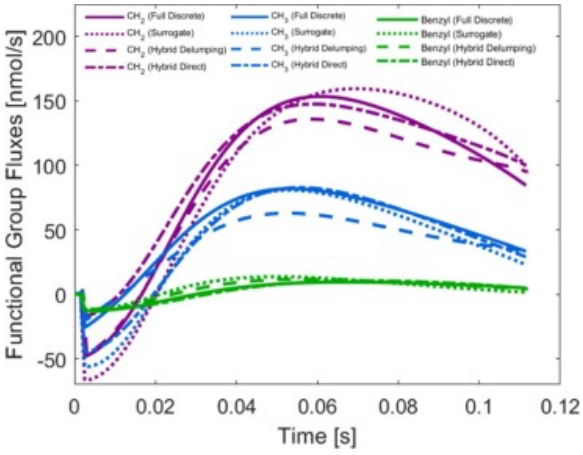

Fig. 17. Flux of chemical functional groups for vaporization into a mixture containing species not present in the physical–chemical surrogate, calculated using the full DCM for the target fuel, the physical–chemical surrogate, CA-DQMoM with delumping and CA-DQMoM with direct prediction of functional groups.

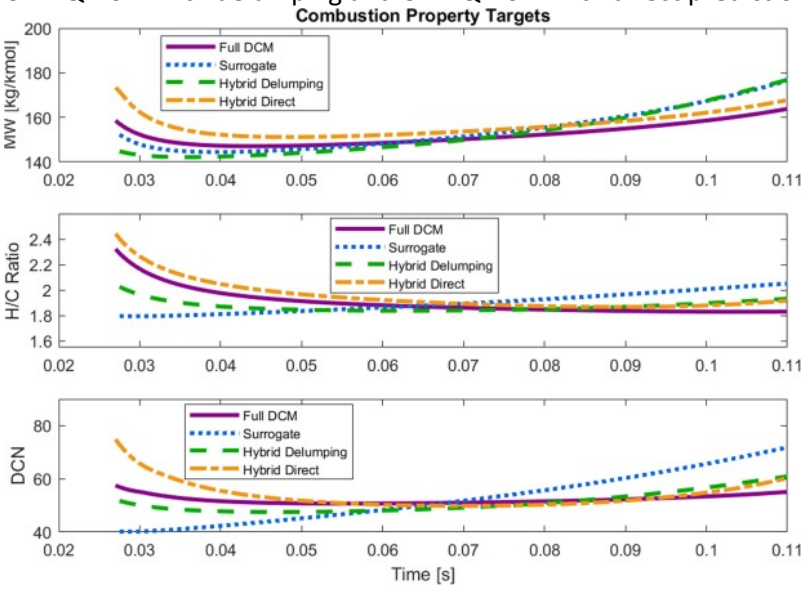

Fig. 18. Chemical properties of the instantaneous flux for vaporization into a mixture containing species not present in the physical–chemical surrogate, calculated using the full DCM for the target fuel, the physical–chemical surrogate, CA-DQMoM with delumping and CA-DQMoM with direct prediction of functional groups.

3.4.4. Computation time

The computation time of all three approximate models are significantly lower than the DCM for the full target fuel, with average reductions of 94.1%, 93.6% and 92.2% for the hybrid method with delumping, the physical-surrogate method and the direct hybrid method, respectively, for test case 1. The CPU time required for the physical–chemical surrogate method (n = 9) is 21.6% lower than the direct hybrid method ($2N$ = 8), even though the hybrid method requires one less ODE and three fewer algebraic equations when using N = 4, as described in Section 2.5. This may be due to the coupled nature of the governing ODEs for the weights and nodes in CA-DQMoM, as seen in Eq. (21). Future efforts to improve the efficiency of the direct hybrid method are warranted, including evaluation of different scaling approaches to reduce the condition number of the DQMoM matrix [50].

4. Conclusions

A unified modeling approach to droplet vaporization and adaptive chemical surrogate formulation appropriate for incorporation in CFD codes is proposed. The previous hybrid modeling approach, which employed CA-DQMoM with delumping for droplet vaporization followed by functional group matching for chemical surrogate formulation, has been modified to eliminate the delumping step and to directly predict the flux of key functional groups to/from the droplet. Although the previous approach is accurate and efficient, this modification extends the applicability of the hybrid approach to a wider range of physical models with no restrictions on the type of nonlinearity, which will be important for future high-pressure applications. To enable CA-DQMoM to directly predict the flux of key functional groups to/from the droplet, a purely mathematical, continuous distribution variable is proposed to replace frequently used continuous distribution variables like molecular weight or normal boiling temperature. The new distribution variable is tailored to correlate key chemical functional groups, in addition to thermophysical and transport properties, and is constructed using an optimization procedure.

A comparison of the two hybrid models to the conventional physical–chemical surrogate approach is also presented. The physical–chemical surrogate is formulated to match the CPTs of the target fuel, as well as its distillation curve, and represents the prevailing approach to accounting for the effects of preferential vaporization. The accuracy of the three approximate methods for multicomponent fuels are evaluated by comparison with the full discrete model for the multicomponent target fuel (which would be prohibitively expensive in a CFD context).

In general, the two hybrid models based on continuous thermodynamics and the physical–chemical surrogate based on a discrete component model all satisfactorily reproduced the instantaneous droplet vaporization/condensation rate. When droplet behavior was dominated by the multicomponent fuel (e.g. boundary conditions of pure air), the hybrid models based on continuous thermodynamics (CA-DQMoM) were more accurate than the physical–chemical surrogate. At times when droplet behavior is dominated by the condensation or re-vaporization of hydrocarbon species that comprise the physical–chemical surrogate itself, the physical–chemical surrogate was slightly more accurate than the hybrid direct model in predicting the vaporization/condensation rate. When the droplet boundary conditions included species that were not part of the physical–chemical surrogate, then the hybrid direct method was more accurate than the physical–chemical surrogate in predicting droplet vaporization/condensation rate.

The instantaneous flux of functional groups to/from the droplet and their CPTs were predicted with higher accuracy by the hybrid models, irrespective of the species boundary conditions to which the droplets were exposed. This is thought to be because the physical–chemical surrogate approach *separately* matches the pre-vaporized CPTs of the target fuel and the distillation curve of the target fuel. Thus, there is no constraint which ensures that the functional group distribution varies along the distillation curve in the same manner as it does for the target fuel. In contrast, in the hybrid direct method, the properties governing vaporization and the functional group distributions are *both* correlated with the optimized distribution variable. This ensures that the functional group fluxes and CPTs of the flux better match those of the target fuel throughout vaporization and should increase the accuracy of Eulerian-phase chemistry in CFD codes. The original hybrid method with delumping is generally the most accurate in its prediction of functional group fluxes and CPTs due to the accuracy of the analytical delumping solution, as discussed elsewhere [19].

The hybrid droplet vaporization-adaptive surrogate model using an optimized distribution variable is a promising method for faithfully representing the impact of multicomponent fuel droplets on gas-phase physics and chemistry in a CFD context. Its capability to accommodate physical models with any type of nonlinearity distinguishes it from the previous CA-DQMoM with delumping hybrid model. Its ability to accurately predict the flux of functional groups and combustion properties throughout vaporization, to produce a small surrogate source term for an Eulerian-phase solver and to accommodate a variety of boundary conditions distinguishes it from the conventional physical–chemical surrogate approach.

CRediT authorship contribution statement

Simcha L. Singer: Conceptualization, Investigation, Methodology, Software, Supervision, Writing - original draft. **Michael P. Hayes:** Investigation, Software, Validation, Writing - review & editing. **Alanna Y. Cooney:** Software, Validation, Writing - review & editing.

Declaration of Competing Interest

The authors declare that they have no known competing financial interests or personal relationships that could have appeared to influence the work reported in this paper.

Acknowledgements

Portions of this research were funded by Marquette University's College of Engineering Legacy Initiative SeedGrant Program and the National Space Grant College and Fellowship Program and the Wisconsin Space Grant Consortium.

References

[1] F.L. Dryer. **Chemical kinetic and combustion characteristics of transportation fuels.** Proc Combust Inst, 35 (2015), pp. 117-144, 10.1016/j.proci.2014.09.008

[2] Lefkowitz JA, Haas FM. Distillation-Resolved Evolution of Key Combustion Properties. In: 10th U. S. Natl. Combust. Meet.; 2017.

[3] R. Xu, H. Wang. **Principle of large component number in multicomponent fuel combustion – a Monte Carlo study.** Proc Combust Inst, 37 (2019), pp. 613-620, 10.1016/j.proci.2018.06.187

[4] H. Wang, R. Xu, K. Wang, C.T. Bowman, R.K. Hanson, D.F. Davidson, *et al.* **A physics-based approach to modeling real-fuel combustion chemistry - I. Evidence from experiments, and thermodynamic, chemical kinetic and statistical considerations.** Combust Flame, 193 (2018), pp. 502-519, 10.1016/j.combustflame.2018.03.019

[5] S.H. Won, F.M. Haas, S. Dooley, T. Edwards, F.L. Dryer. **Reconstruction of chemical structure of real fuel by surrogate formulation based upon combustion property targets.** Combust Flame, 183 (2017), pp. 39-49, 10.1016/j.combustflame.2017.04.032

[6] D. Kim, J. Martz, A. Abdul-Nour, X. Yu, M. Jansons, A. Violi. **A six-component surrogate for emulating the physical and chemical characteristics of conventional and alternative jet fuels and their blends.** Combust Flame, 179 (2017), pp. 86-94, 10.1016/j.combustflame.2017.01.025

[7] O.S. Abianeh, M.A. Oehlschlaeger, C.-J. Sung. **A surrogate mixture and kinetic mechanism for emulating the evaporation and autoignition characteristics of gasoline fuel.** Combust Flame, 162 (2015), pp. 3773-3784, 10.1016/j.combustflame.2015.07.015

[8] N.S. Surrogate. **Formulation Based on Chemical Functional Group Analysis.** University of South Carolina (2019)

[9] B.L. Smith, T.J. Bruno. **Improvements in the measurement of distillation curves. 4. Application to the aviation turbine fuel jet-A.** Ind Eng Chem Res, 46 (2007), pp. 310-320, 10.1021/ie060938m

[10] L. Qiu, R.D. Reitz. **An investigation of thermodynamic states during high-pressure fuel injection using equilibrium thermodynamics.** Int J Multiph Flow, 72 (2015), pp. 24-38, 10.1016/j.ijmultiphaseflow.2015.01.011

[11] S.L. Kokjohn, R.M. Hanson, D.A. Splitter, R.D. Reitz. **Fuel reactivity controlled compression ignition (RCCI): a pathway to controlled high-efficiency clean combustion.** Int J Engine Res, 12 (2011), pp. 209-226, 10.1177/1468087411401548

[12] A.Y. Cooney, S.L. Singer. **A hybrid droplet vaporization-chemical surrogate approach for emulating vaporization, physical properties, and chemical combustion behavior of multicomponent fuels.** Proc Combust Inst, 3 (2019), pp. 3229-3236

[13] A.Y. Cooney, S.L. Singer. **Modeling Multicomponent Fuel Droplet Vaporization with Finite Liquid Diffusivity using Coupled Algebraic-DQMoM with Delumping.** Fuel, 212 (2018), pp. 554-565, 10.1016/j.fuel.2017.10.056

[14] Krishnasamy A, Reitz RD, Willems W, Kurtz E. Surrogate Diesel Fuel Models for Low Temperature Combustion. SAE 2013 World Congr. Exhib., 2013, p. 2013-01–1092. https://doi.org/10.4271/2013-01-1092.

[15] Y. Ra, R.D. Reitz. **A combustion model for multi-component fuels using a physical surrogate group chemistry representation (PSGCR).** Combust Flame, 162 (2015), pp. 3456-3481, 10.1016/j.combustflame.2015.05.014

[16] Y. Zhang, M. Jia, P. Wang, Y. Chang, P. Yi, H. Liu, *et al.* **Construction of a decoupling physical–chemical surrogate (DPCS) for practical diesel fuel.** Appl Therm Eng, 149 (2019), pp. 536-547, 10.1016/j.applthermaleng.2018.12.053

[17] P. Wang, M. Jia, Y. Zhang, G. Xu, Y. Chang, Z. Xu. **Development of a decoupling physical-chemical surrogate (DPCS) model for simulation of the spray and combustion of multi-component biodiesel fuels.** Fuel, 240 (2019), pp. 16-30, 10.1016/j.fuel.2018.11.134

[18] L. Qiu, Y. Wang, R.D. Reitz. **On regular and retrograde condensation in multiphase compressible flows.** Int J Multiph Flow, 64 (2014), pp. 85-96, 10.1016/j.ijmultiphaseflow.2014.05.004

[19] S.L. Singer. **Direct quadrature method of moments with delumping for modeling multicomponent droplet vaporization.** Int J Heat Mass Transf, 103 (2016), pp. 940-954

[20] A.Y. Cooney, S.L. Singer. **Modeling high-pressure multicomponent droplet vaporization using quadrature moment methods with delumping and the Peng-Robinson equation of state.** ILASS (2018)

[21] D.-Y. Peng, D.P. Robinson. **A new two-constant equation of state.** Ind Eng Chem, Fundam, 15 (1976), pp. 59-64

[22] G.J. Brereton. **A discrete multicomponent temperature-dependent model for the evaporation of spherical droplets.** Int J Heat Mass Transf, 60 (2013), pp. 512-522, 10.1016/j.ijheatmasstransfer.2013.01.037

[23] B. Abramzon, W.A. Sirignano. **Droplet vaporization model for spray combustion calculations.** Int J Heat Mass Transf, 32 (1989), pp. 1605-1618, 10.1016/0017-9310(89)90043-4

[24] W. Sirignano. **Fluid dynamics and transport of droplets and sprays.** Cambridge University Press, New York (2010)

[25] L.A. Dombrovsky, S.S. Sazhin. **A simplified non-isothermal model for droplet heating and evaporation.** Int Commun Heat Mass Transf, 30 (2003), pp. 787-796, 10.1016/S0735-1933(03)00126-X

[26] Laurent C. Développement et validation de modèles d'évaporation multi-composant, Ph.D. Thesis. Universite de Toulouse, l'Institut Supérieur de l'Aéronautique et de l'Espace; 2008.

[27] Yaws CL. Yaws' Thermophysical Properties of Chemicals and Hydrocarbons. Knovel; 2010.

[28] G.L. Hubbard, V.E. Denny, A.F. Mills. **Droplet evaporation: Effects of transients and variable properties.** Int J Heat Mass Transf, 18 (1975), pp. 1003-1008

[29] C. Laurent, G. Lavergne, P. Villedieu. **Continuous thermodynamics for droplet vaporization: comparison between Gamma-PDF model and QMoM.** Comptes Rendus Mec, 337 (2009), pp. 449-457, 10.1016/j.crme.2009.06.004

[30] L. Zhang, S.C. Kong. **Modeling of multi-component fuel vaporization and combustion for gasoline and diesel spray.** Chem Eng Sci, 64 (2009), pp. 3688-3696, 10.1016/j.ces.2009.05.013

[31] D.L. Marchisio, R.O. Fox. **Solution of population balance equations using the direct quadrature method of moments.** J Aerosol Sci, 36 (2005), pp. 43-73, 10.1016/j.jaerosci.2004.07.009

[32] W.L.H. Hallett, N.V. Legault. **Modelling biodiesel droplet evaporation using continuous thermodynamics.** Fuel, 90 (2011), pp. 1221-1228, 10.1016/j.fuel.2010.11.035

[33] S. Yang, R.D. Reitz. **Integration of a continuous multi-component fuel evaporation model with an improved G-equation combustion and detailed chemical kinetics model with application to GDI engines.** SAE Tech Pap Ser (2009), pp. 01-0722, 10.4271/2009-01-0722

[34] R. McGraw. **Description of aerosol dynamics by the quadrature method of moments.** Aerosol Sci Technol, 27 (1997), pp. 255-265, 10.1080/02786829708965471

[35] T.M. Lovestead, J.L. Burger, N. Schneider, T.J. Bruno. **Comprehensive Assessment of Composition and Thermochemical Variability by High Resolution GC/QToF-MS and the Advanced Distillation-Curve**

Method as a Basis of Comparison for Reference Fuel Development. Energy Fuels, 30 (2016), pp. 10029-10044, 10.1021/acs.energyfuels.6b01837

[36] J. Cai, J.M. Prausnitz. **Stability criteria for a polydisperse system.** Fluid Phase Equilib, 206 (2003), pp. 41-59, 10.1016/S0378-3812(02)00312-6

[37] T. Runge, M. Teske, C. Polymeropoulos. **Low Temperature Vaporization of JP-4 and JP-8 Fuel Droplets.** At Sprays, 8 (1998), pp. 25-44

[38] Edwards T. Reference jet fuels for combustion testing. AIAA SciTech Forum - 55th AIAA Aerosp. Sci. Meet., 2017;17:12772–829. https://doi.org/10.2514/6.2017-0146.

[39] P.B. Govindaraju, M. Ihme. **Group contribution method for multicomponent evaporation with application to transportation fuels.** Int J Heat Mass Transf, 102 (2016), pp. 833-845, 10.1016/j.ijheatmasstransfer.2016.06.079

[40] H. Nomura, Y. Ujiie, H.J. Rath, J. Sato, M. Kono. **Experimental study on high-pressure droplet evaporation using microgravity conditions.** Symp Combust, 26 (1996), pp. 1267-1273, 10.1016/S0082-0784(96)80344-4

[41] R.N. Dahms, J.C. Oefelein. **The significance of drop non-sphericity in sprays.** Int J Multiph Flow, 86 (2016), pp. 67-85, 10.1016/j.ijmultiphaseflow.2016.07.010

[42] C. Yan, S.K. Aggarwal. **A high-pressure droplet model for spray simulations.** J Eng Gas Turbines Power, 128 (2006), p. 482, 10.1115/1.1915390

[43] H. Zhang, V. Raghavan, G. Gogos. **Subcritical and supercritical droplet evaporation within a zero gravity environment; on the discrepancies between theoretical and experimental results.** Int J Spray Combust Dyn, 1 (2009), pp. 317-338, 10.1260/175682709789141555

[44] R.C. Striebich, L.M. Shafer, R.K. Adams, Z.J. West, M.J. DeWitt, S. Zabarnick. **Hydrocarbon group-type analysis of petroleum-derived and synthetic fuels using two-dimensional gas chromatography.** Energy Fuels, 28 (2014), pp. 5696-5706, 10.1021/ef500813x

[45] T.J. Bruno. **Improvements in the measurement of distillation curves. 1. A composition-explicit approach.** Ind Eng Chem Res, 45 (2006), pp. 4371-4380, 10.1021/ie051393j

[46] D. Kim, J. Martz, A. Violi. **A surrogate for emulating the physical and chemical properties of conventional jet fuel.** Combust Flame, 161 (2014), pp. 1489-1498, 10.1016/j.combustflame.2013.12.015

[47] K.L. Berrier, C.E. Freye, M.C. Billingsley, R.E. Synovec. **Predictive modeling of aerospace fuel properties using comprehensive two-dimensional gas chromatography with time-of-flight mass spectrometry and partial least squares analysis.** Energy Fuels, 34 (2020), pp. 4084-4094, 10.1021/acs.energyfuels.9b04108

[48] M. Wissink, R.D. Reitz. **Direct dual fuel stratification, a path to combine the benefits of RCCI and PPC.** SAE Int J Engines, 8 (2015), pp. 878-889, 10.4271/2015-01-0856

[49] A.G. Abdul Jameel, N. Naser, G. Issayev, J. Touitou, M.K. Ghosh, A.H. Emwas, *et al.* **A minimalist functional group (MFG) approach for surrogate fuel formulation.** Combust Flame, 192 (2018), pp. 250-271, 10.1016/j.combustflame.2018.01.036

[50] F.P. Santos, P.L.C. Lage, C.E. Fontes. **Quadrature-based moment methods for solving the population balance equation.** Brazilian J Chem Eng, 30 (2013), pp. 643-656